College of Engineering

Mesoporous carbide-derived carbon with porosity tuned for efficient adsorption of cytokines

Gleb Yushin, Elizabeth N. Hoffman, Michel W. Barsoum, Yury Gogotsi *

Department of Materials Science and Engineering and A.J. Drexel Nanotechnology Institute, Drexel University, Philadelphia, Pennsylvania, 19104, USA

Carol A. Howell, Susan R. Sandeman, Gary J. Phillips, Andrew W. Lloyd and Sergey V. Mikhalovsky

School of Pharmacy and Biomolecular Sciences, University of Brighton, Moulsecoomb, Brighton BN2 4GJ, UK

* To whom correspondence should be addressed at: E-mail: gogotsi@drexel.edu

Biocompatible porous carbons can be used for the purification of various bio-fluids, including the cleansing blood of inflammatory mediators in conditions such as sepsis or auto-immune diseases. Here we show that the control of pore size in carbons is a key factor to achieving efficient removal of cytokines. In particular, the surface area accessible by the protein governs the rate and effectiveness of the adsorption process. We demonstrate that novel mesoporous carbon materials synthesized from ternary MAX-phase carbides can be optimized for efficient adsorption of large inflammatory proteins. The synthesized carbons, having tunable pore size with a large volume of slit-shaped mesopores, outperformed all other materials or methods in terms of efficiency of TNF-α removal and the results are comparable only with highly specific antibody-antigen interactions.

The worldwide occurrence of sepsis with over 18 million cases recorded annually and the absence of efficient drug-based therapies, make this systemic inflammatory response to infection one of the leading causes of death (1). Severe sepsis, which accounts for over 17 % of the total sepsis cases, and having a current mortality rate 30-40 %, is responsible for the death of 1,500 people/day worldwide, on a scale comparable to lung and breast cancer (~ 2,700 and ~ 1,100 people /day, respectively) (1,2). From an economic perspective, sepsis places a significant burden on healthcare systems, costing over $ 17 billion / year in the US alone (3). The inflammatory response to various bodily insults is driven by a complex network of inflammatory mediators, these consist mainly of proteins called cytokines (4-6). Cytokine removal from blood may help to bring under control the unregulated pro- and anti-inflammatory processes driving sepsis. Therapies aimed at the simultaneous reduction of cytokines across a wide range of molecular sizes might, therefore, prove more effective than drugs directed against a single or a few inflammatory mediators (5-7). Hemofiltration or hemoadsorption could allow extracorporeal removal of these inflammatory cytokines to an extent that is sufficient to strongly reduce the inflammatory response. While both sieving and adsorption could play a role in hemofiltration, the adsorption characteristics of the filter material are generally believed to be a dominant factor in membrane efficiency. Adsorption can remove toxins without introducing other substances into the blood. Therefore, hemoadsorption might have advantages over hemofiltration, having the same or better efficiency in the treatment of inflammatory diseases, being of lower cost and offering considerably better comfort for patients during and after the treatments (8).

Activated carbons (ACs), known for over three thousand years, still remain the most powerful conventional adsorbents (8), mainly due to their highly developed porous structure and large surface area. Most of the specially purified ACs prepared from synthetic polymers show excellent biocompatibility and do not require special coatings for direct contact with blood (8,9). However, despite extensive studies and improvements in the activation processes, little control over the pore structure has been achieved. Even advanced ACs show limited performance in adsorbing large inflammatory proteins, mostly due to the limited surface area accessible to the adsorbate. Templating has previously been used to increase the volume fraction of the larger pores (10-12). For example, porous carbon was prepared by introducing carbon into the pores of alumina or silica substrates and subsequently dissolving the oxide template by acidic treatment. Apart from cost issues, the resulting carbon generally demonstrates poor mechanical integrity and near-spherical shape of the pores with the bottlenecks that do not allow large molecules to be adsorbed inside the bulk of the particles. In principle, it follows that interconnected slit-shaped pores of an optimized size would be more advantageous for the discussed application. Small particles (< 100 nm) would offer a larger external surface, but they cannot be used in most of the biomedical applications due to difficulties of filtering them from the biofluids. The pore size in other porous carbon materials, such as carbon nanotubes (CNT), is very difficult to control and tune to the desired values. Most CNTs have a low specific surface area (SSA) and agglomeration of CNT into ropes, particularly when they are brought in contact with biofluids, generally significantly reduces their accessible surface area.

Carbon produced by etching of metal(s) from metal carbides and called carbide derived carbon (CDC) has recently been shown to offer great potential for controlling the size of micropores (0.4 – 2 nm) (13). CDCs are generally produced by chlorination of carbides in the 200-1200°C temperature range. Metals and metalloids are removed as chlorides, leaving behind a collapsed noncrystalline carbon with up to 80% open pore volume. The detailed nature of the porosity - average size and size distribution, shape, and total specific surface area (SSA) - can be tuned with high sensitivity by the judicious selection of the precursor carbide (composition, lattice type, etc.) (13-16) and chlorination temperature (13). However, only tuning of microporosity (0.4-2 nm) has been demonstrated in CDCs so far. In this paper we demonstrated a method to produce porous carbons with controlled volume and surface area of slit-shaped mesopores (2-50 nm) of certain size by CDC synthesis from selected ternary (MAX-phase) carbides (17) and investigated the effect of pore structure on removal of cytokines from blood.

Results and discussion

Porosity characterization. Figure 1 shows the N_2 sorption isotherms of CDCs (Fig. 1A) and commercial carbon samples (Fig. 1B). All the samples, except Adsorba 300C, demonstrate type IV isotherm according to the Brunauer classification (18) with a characteristic hysteresis, suggesting the presence of mesopores (pores with size in the 2-50 nm range). CDCs from both Ti_2AlC (Fig. 1A) and Ti_3AlC_2 (not shown) demonstrate similar trends as the temperature of synthesis changes. The volume of N_2 adsorbed in the porous structure of CDC prepared at lower temperature (600 °C) approaches half of the maximum values at low relative pressure (P/P_0). The steep slope of the adsorption curve at P/P_0 values approaching 1, associated with capillary condensation in mesopores, is

quite short, suggesting a small mesopore volume (19). The N_2 sorption behavior changes dramatically at intermediate (~ 800 °C) chlorination temperatures. The total volume of adsorbed N_2 more than doubles; an increase is observed over the whole P/P_0 range, indicating a significant increase in both the total and mesopore volume. The level of adsorption-desorption hysteresis, and the steep slope as P/P_0 approaches unity also increases substantially, in agreement with the suggested increase in the relative volume of mesopores. As the synthesis temperature increases to 1200 °C, the volume of adsorbed N_2 further increases in the P/P_0 range of up to ~ 0.8, but becomes lower at higher P/P_0 values (Fig. 1A). Such changes in the isotherm shape indicate the reduction in the relative volume of larger mesopores.

The pore size distribution (PSD) curves calculated in the 1.5-36 nm range for all the studied samples from the N_2 isotherms (Fig. 2) fully support the aforementioned conclusions. The CDC samples formed at low temperature (600° C) have a very low volume of mesopores, particularly those above 10 nm (Figs. 2B and 2F). At the intermediate synthesis temperatures (800° C), the PSD becomes wider and shifts to higher pore-size values (Figs. 2C and 2G). These samples clearly have the largest volume of mesopores above 5 nm. At the high chlorination temperature of 1200 °C the total CDC mesopore volume remains relatively high (Fig. 2D and 2H). It is in fact higher than the total pore volume of many activated carbon samples, including Adsorba 300C (Fig. 2A). However, most of the mesopores in these samples are below 4-5 nm. Adsorba 300C has the smallest volume of mesopores and is almost purely microporous carbon. The PSD of the CXV sample (Fig. 2E) is close to that of an average of CDC samples produced at high

and intermediate temperatures. The porosity data for all the studied samples are summarized in Table S1 (Supplementary Information).

While Ar sorption is not a very efficient technique to study the large mesopores, it gives more accurate PSD results for small (< 4 nm) pore values, mainly due to argon's smaller atomic size, the absence of quadrupole moment (which can potentially lead to localized adsorption as in case of N_2) and its weaker interactions with carbon adsorbents. The PSD of the studied samples in the 0.4 - 4 nm range obtained from Ar sorption isotherms (Supplementary Information, Fig. S1) revealed details of the samples' microporosity. Similar to Adsorba 300C, both CDC samples produced at 600 °C have the majority of pores below 2 nm in width. As the CDC synthesis temperature increases, the average size of the pores in the 0.4 - 4 nm range increases as well (Fig. S1). However, above 800 °C, pores in the 2-4 nm range have a tendency to grow on the account of the micropores, forming a large volume of ~ 3 nm pores at 1200 °C. The PSD of the CXV sample is close to the average between the CDC samples formed at 800 and 1200 °C.

Transmission electron microscopy. Transmission electron microscopy (TEM) revealed disordered microstructure of all the studied carbons. The degree of disorder was different between the carbons. Both CDCs formed at 600 °C demonstrate completely amorphous structure, without any graphite fringes visible (Fig. 3A). Increasing the CDC processing temperature to 800 °C resulted in the formation of short curved graphene structures, considered turbostratic carbon (Fig. 3B). At 1200 °C TEM detected markedly increased ordering and the formation of long and thin (1-3 graphene sheets) graphite ribbons (Fig. 3C). At the edge of the particles, ribbons with up to 10 graphene layers were found (Fig.

3C). The microstructure of Adsorba 300C sample was found to be highly amorphous, (Fig. 3D) while that of the CXV carbon (Fig. 3E), turbostratic.

Our previous studies have shown that the observed evolution of ordering within the carbon structure with the chlorination temperature is quite common for most of the CDCs obtained from both ternary and binary carbides (20). The changes in the PSDs correlate to changes in the CDC microstructure. The low mobility of the carbon atoms at the low chlorination temperatures resulted in the formation of a uniform amorphous structure (Fig. 3A) with small micropores (Figs. 2B, 2F, S1B, S1F). At higher synthesis temperatures, higher carbon mobility allowed for the formation of graphitic ribbon networks (Fig. 3C), with mesopores forming between the graphene ribbons and micropores in the imperfections of the graphitic ribbons or within the remaining disordered carbon (Figs. 2D, 2H, 1SD, 1SH). At the intermediate temperature of 800 °C, the mobility of carbon was high enough to allow for a redistribution of carbon atoms into defective graphene sheets and the collapse of several sheets into stacks forming mesopores between them. However, the mobility was still too low to allow uniform linking between the turbostratic ribbons, resulting in a wide distribution of mesopores (Figs. 2C, 2G). Note, that since precise determination of non-spherical pores in disordered non-planar particles is not possible using TEM, we relied on gas sorption measurements for the PSD determination.

Cytokine adsorption. Figure 4 compares efficiency of removal of two selected cytokines (tumor necrosis factor alpha (TNF-α) and interleukin-6 (IL-6)) from human plasma using the investigated carbons. Adsorption of TNF-α is known to be the most challenging task, probably due to a large size (> 9.4 nm) of the trimeric (most common) form of this

cytokine (21). Adsorba 300C and CDC produced at 600°C, which have small pores, did not noticeably change the protein concentration over time. CDC produced at 1200 °C and CXV also demonstrated a limited success in the adsorption of TNF-α, decreasing its concentration by about 40 % after one hour of adsorption (Fig. 4A), similar to that observed in advanced porous carbon hemoadsorption systems (22). In contrast, both CDC samples prepared at 800 °C decreased the protein concentration by over 13 times in this time period. To the best of our knowledge, in these experiments CDCs outperformed any other material or method for the efficient removal of TNF-α, and the results are comparable only to highly specific antibody-antigen interactions (23, 24).

Adsorption of the smaller cytokine IL-6 by most of the studied carbons was noticeably higher, but demonstrated similar trends (Fig. 4B). Strictly microporous Adsorba 300C was clearly inefficient. However, CDCs prepared at 600 °C, having a limited amount of mesopores (pores 2-50 nm), adsorbed 66 to 77 % of the cytokines initially present in the solution in one hour. The CDCs produced at 1200° C demonstrated 97-98.5 % adsorption, which is comparable to the CXV sample, capable of adsorbing ~ 99 %. The CDCs prepared from Ti_2AlC at 800 °C, having the most developed mesoporosity decreased IL-6 concentration by ~ 99.8 %; the remaining IL-6 was close to the detection limit of the ELISA used.

A clear dependence of protein removal efficiency on the PSDs of the porous carbons is seen when protein adsorption is plotted as a function of the carbons' accessible surface area, which is approximated as the SSA of pores exceeding the smallest protein dimension in size (Fig. 5). Dimensions of the investigated cytokines were considered to be: 9.4 x 9.4 x 11.7 nm (trimer of TNF-α) (21), 5.5 x 5.5 x 7.7 nm (IL-1β) (25), 5 x 5 x

12.2 nm (IL-6) (26), 4 x 4 x 9 nm (IL-8) (27). The larger the surface areas of the porous carbons accessible to a given cytokine (SSAacc), the more cytokines were adsorbed at a given time (Figs. 5A, 5B, 5C, 5D). Some scattering in the results obtained could be explained by experimental errors in the estimation of the cytokine concentration and the carbon PSD. Depending on the cytokine and its initial concentration, values of the SSA_{acc} above 50-100 m^2/g were generally sufficient for fast and efficient cytokine removal. The relatively short and small IL-1β and IL-8 cytokines diffused so rapidly into the carbon pores that 5 min was sufficient to adsorb most of these proteins by carbons with SSA_{acc} exceeding 50 m^2/g (Figs. 5B and 5D). The existence of larger channels within these carbons should have further accelerated the adsorption process. IL-6 demonstrated slower adsorption (Fig. 5C), probably due to its longer dimensions and hence slower diffusion within the carbon pore structure. The TNF-α trimer, the largest adsorbate, demonstrated a further decrease in adsorption rate (Fig. 5A) as the amount of pores, exceeding three times the adsorbate size needed for fast diffusion, was limited (Figs. 2C and 2G).

Historically, in medical sciences and applied medicine, activated carbons are considered to be high SSA carbons of ultra purity. Differentiation of activated carbons with respect to difference in their PSD is uncommon. In fact, the same carbon materials are often used for adsorption of various species, from gases to organic molecules. However, since most commercial medical grade activated carbons, including Adsorba, are primarily microporous (Figs. 2A, 1SA), adsorption of inflammatory mediators with size exceeding 2 nm could only take place on the particles' surface (Fig. 6A). The calculated SSA of spherical carbon particles with a 10 μm diameter and 50 % porosity is only ~ 0.3 m^2/g, which is much smaller than the 386 - 406 m^2/g SSA of mesopores (2-50

nm) in the CDCs produced at 800 °C. It is thus not too surprising that clinical trials of commercial extracorporeal adsorption systems did not show significantly decreased mortality in patients with sepsis (28,29). Large biological molecules can move through pores of appropriate size, as translocation of DNA through a nanotube demonstrated recently (30), and be adsorbed in the bulk of the adsorbent particles (Fig. 6B). Pore size control is thus a key issue for achieving highly-efficient removal of large cytokines from blood plasma. Engineering of novel nanostructured CDC adsorbents, with rationally optimized porosity may provide a solution for extracorporeal adsorption systems and save the lives of people suffering severe sepsis. Similar approaches could be used for the selective adsorption of other large organic molecules and possibly viruses for other bio-related or medical applications.

The CDC method presented here, together with the unique layered structure of the ternary MAX-phase carbide precursors used here, has made it possible to synthesize mesoporous carbons with large volumes and surface areas of slit-shaped mesopores. Based on this work it appears that not only micropores (0.4-2 nm) but also mesopores (2-50 nm) can be tuned in a controlled way by extraction of metals from carbides, providing a mechanism for the optimization of adsorption systems for selective sorption of a large variety of biomolecules.

Materials and Methods

Materials. CDCs were synthesized from commercially available (3-ONE-2, Inc, NJ, US) and produced at Drexel University powders of Ti_2AlC and Ti_3AlC_2 by the reaction with pure chlorine (99.5%, BOC gases) at 600, 800 and 1200°C. Both carbides belong to the MAX-phase group of ternary carbides, having a layered hexagonal structure with carbon

atoms positioned in basal planes and separated by 0.68 nm (Ti2AlC) or alternating layers of 0.31 and 0.67 nm (Ti3AlC2) (31). The CDCs produced from these carbides are known to posses slit-shaped open pores (13,32,33). The average particle size of the carbide samples used in our experiments was ~ 10 μm, as measured using a particle size analyzer (Horiba LA-910, Japan). For CDC synthesis, the selected carbide powder was placed onto a quartz sample holder and loaded into the hot zone of a horizontal quartz tube furnace. Prior to heating, the tube (~ 30 mm in diameter) was purged with high purity Ar (BOC Gases, 99.998%) for 30 minutes at a flow rate of 100 sccm. Once the desired temperature was reached and stabilized, the Ar flow was stopped and a 3-hour chlorination began with Cl_2 flowing at a rate of 10 sccm. After the completion of the chlorination process, the samples were cooled down under a flow of Ar (40 sccm) for about five hours to remove any residual chlorine or metal chlorides from the pores, and taken out for further analyses. In order to avoid a back-stream of air, the exhaust tube was connected to a bubbler filled with sulphuric acid. A detailed description of the chlorination apparatus used in this study can be found elsewhere (20).

The sorption performance of the CDCs was compared with that of Adsorba 300C and CXV carbon adsorbents. Adsorba 300C is an activated carbon produced by Norit from peat, and coated with a 3-5 μm thick cellulose membrane for better hemocompatibility. It is commercially used in adsorbent-assisted extracorporeal systems manufactured by Gambro, Sweden. CXV is an activated carbon obtained from CECA (subsidiary of Arkema, France), known to be extremely efficient for cytokine removal applications and thus used as a benchmark reference.

Characterization. The structure of the CDCs was investigated using high-resolution transmission electron microscopy (HRTEM). The TEM samples were prepared by two minutes sonication of the CDC powder in isopropanol and deposition on the lacey-carbon coated copper grid (200 mesh). A field-emission TEM (JEOL 2010F, Japan) with an imaging filter (Gatan GIF) was used at 200 kV.

The porosity of CDCs was studied using automated micropore gas analyzers Autosorb-1 and Nova (Quantachrome Instruments, USA). The N_2 and Ar sorption isotherms were obtained at liquid nitrogen temperature (-196 ^{o}C) in the relative pressure P/P_0 range of about $8 \cdot 10^{-7}$ to 1 and $2 \cdot 10^{-2}$ to 1, respectively. The isotherms were analyzed using Brunauer–Emmet-Teller (BET) equation and non-local density functional theory (NLDFT) (18,19,34,35) to reveal the SSA and pore-size distributions (PSD) of the CDCs. The SSAs calculated using BET and DFT theory are referred to as BET-SSA and DFT-SSA, respectively. A difference in absolute values between BET-SSA and DFT-SSA is expected, as both types of calculations are based on different assumptions, which might not be justified with the utmost accuracy for all the materials under study. Quantachrome Instruments data reduction software Autosorb v.1.50 (1 9) was employed for the porosity analysis. Slit-shaped pores were assumed for the calculations.

Cytokine adsorption experiments. Fresh frozen human plasma (NBS, UK) was defrosted and spiked with the recombinant human cytokines (TNF-α, IL-1β, IL-6, and IL-8; all obtained from BD Biosciences, US) at a concentration of about 1000, 500, 5000, and 500 pg/ml, respectively. These levels are comparable with the concentrations measured in the plasma of patients with sepsis (36-38). Carbon adsorbents (0.02 g) were equilibrated in phosphate buffered saline (PBS) (0.5 ml) overnight prior to removal of

PBS and addition of 800 μl of spiked human plasma. Controls consisted of spiked plasma with no adsorbent present. Adsorbents were incubated at 37 °C while shaking (90 rpm). At 5, 30 and 60 min time points, samples were centrifuged (125g) and the supernatant collected and stored at -20 °C prior to ELISA (BD Biosciences) analysis for the presence of cytokines. Samples were diluted 1:4 (TNF-α, IL-8, IL-1β) and 1:10 (IL-6) in assay diluent prior to analysis.

Acknowledgements

This research was supported by the US National Science Foundation. TEM studies were performed at Penn Regional Nanotechnology Facility, University of Pennsylvania. Additional material characterization was performed at the Centralized Materials Characterization Facility of the A.J. Drexel Nanotechnology Institute. E. Hoffman was supported by the NSF IGERT grant # DGE-0221664.

Figures:

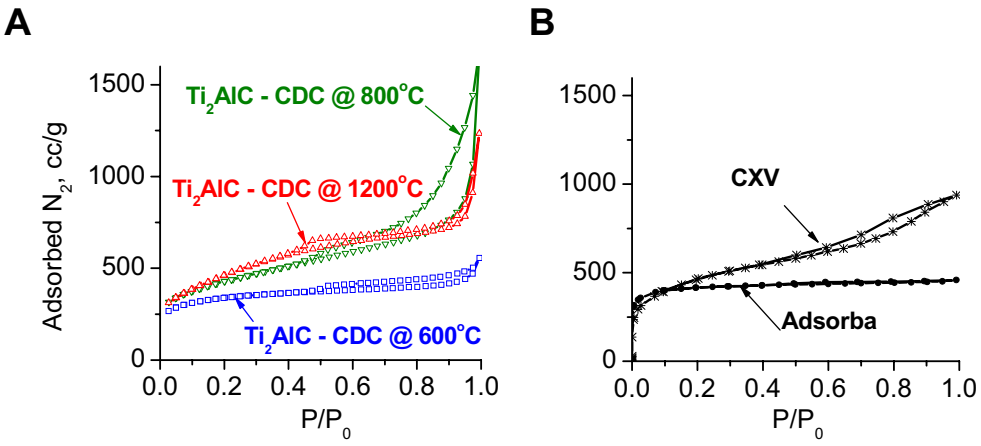

Fig. 1. Nitrogen sorption isotherms. (A) Ti_2AlC CDC, (B) CXV and Adsorba samples. N_2 isotherms for Ti_3AlC_2 CDC are very similar to the isotherms for Ti_2AlC CDC synthesized at identical temperatures.

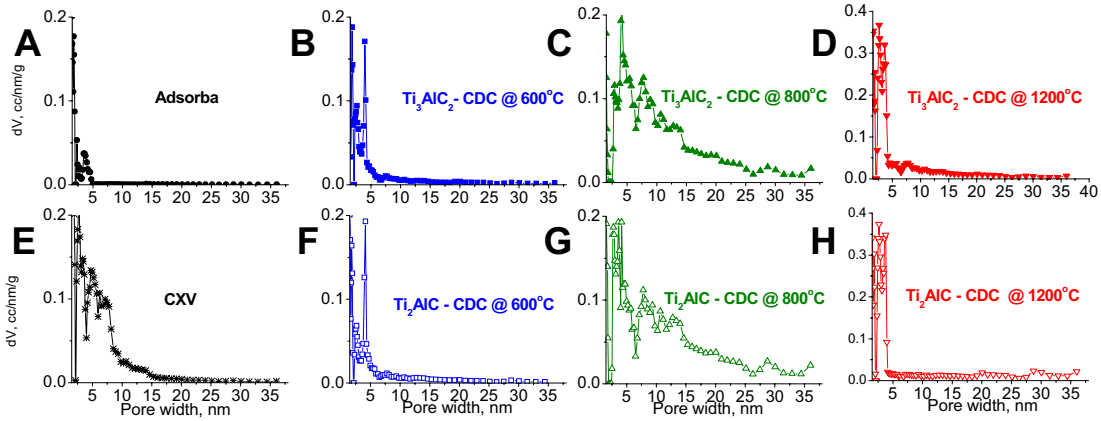

Fig. 2. Distribution of pore sizes of porous carbons in the 1.5 - 36 nm range obtained from N_2 sorption isotherms. (A) Adsorba, (B-D) CDC produced from Ti_3AlC_2 at 600, 800, and 1200° C, (E) CXV, (F-H) CDC produced from Ti_2AlC at 600, 800, and 1200° C.

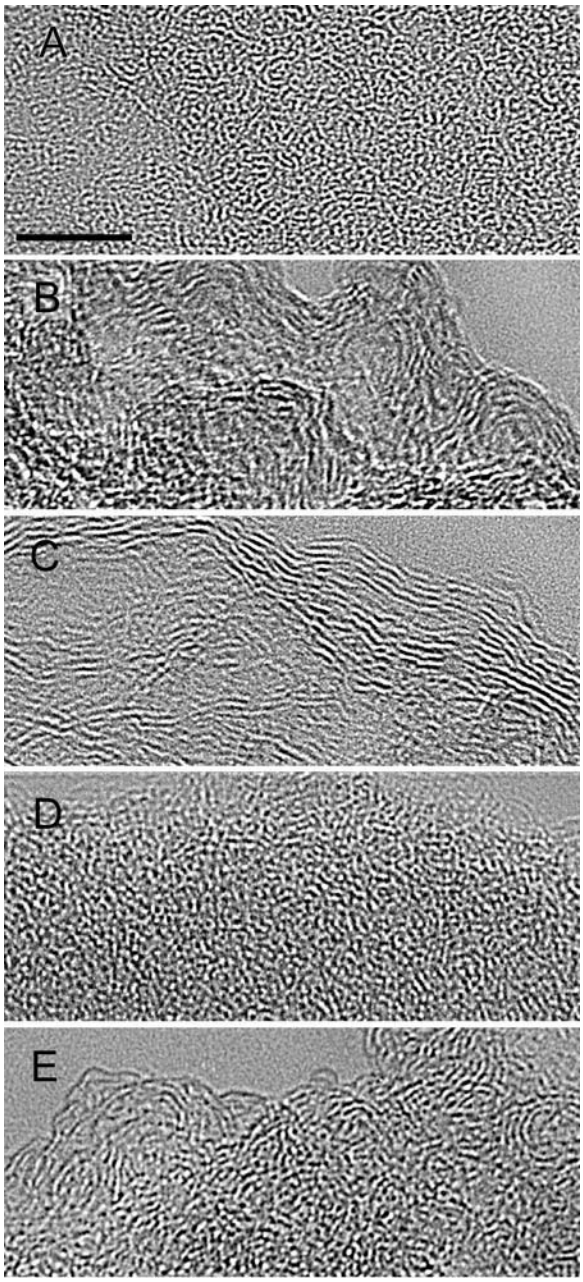

Fig. 3. Transmission electron microscopy of porous carbon samples. (A-C) CDC produced from Ti_2AlC at 600, 800, and 1200° C, (D) Adsorba, (E) CXV. The structure of Ti_3AlC_2 CDC replicates the one for Ti_2AlC CDC if synthesized at identical temperatures. Scale bar = 5 nm.

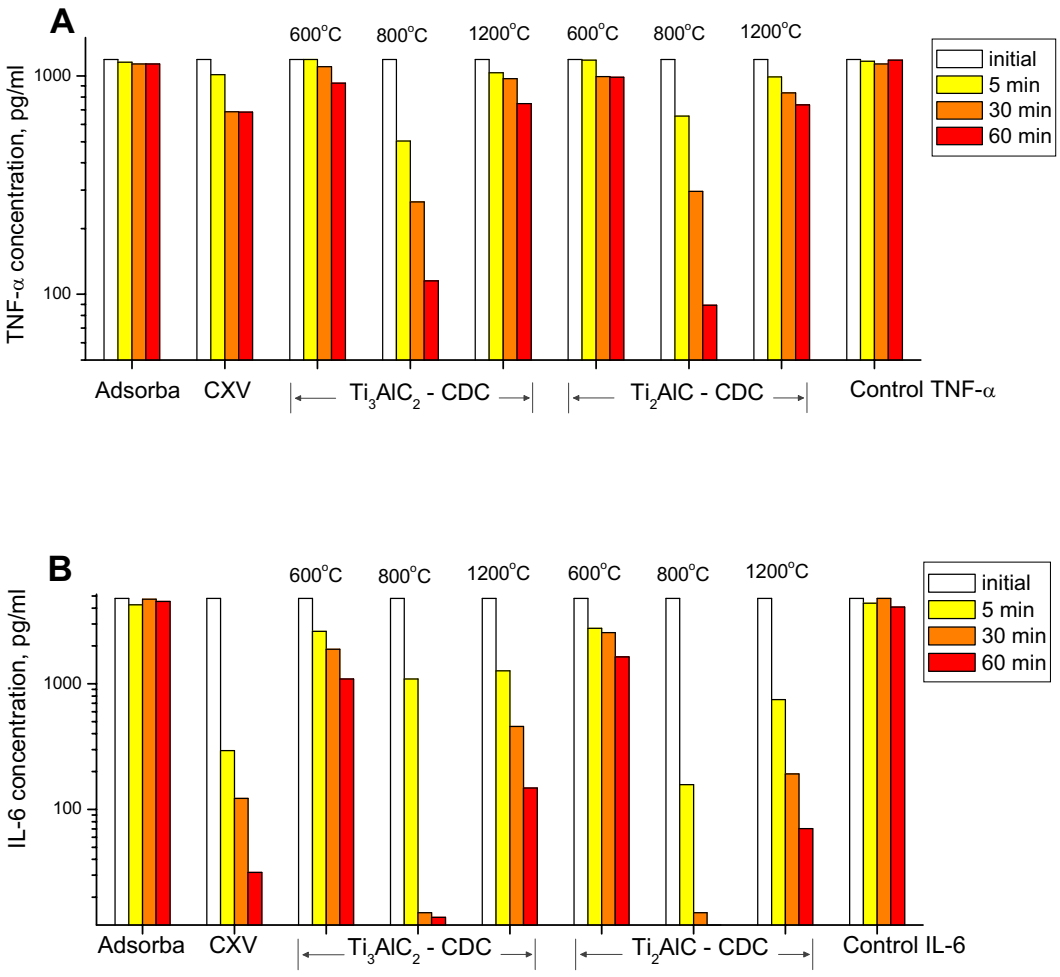

Fig. 4. Comparison of the porous carbons efficiency in the cytokine removal from human blood plasma. (A) Concentration of TNF-α in the plasma solution initially and after 5, 30, and 60 minutes of adsorption. (B) Similar changes in IL-6 concentration. Both CDC samples produced at 800° C and having developed mesoporosity outperformed other materials in the efficiency of cytokines removal.

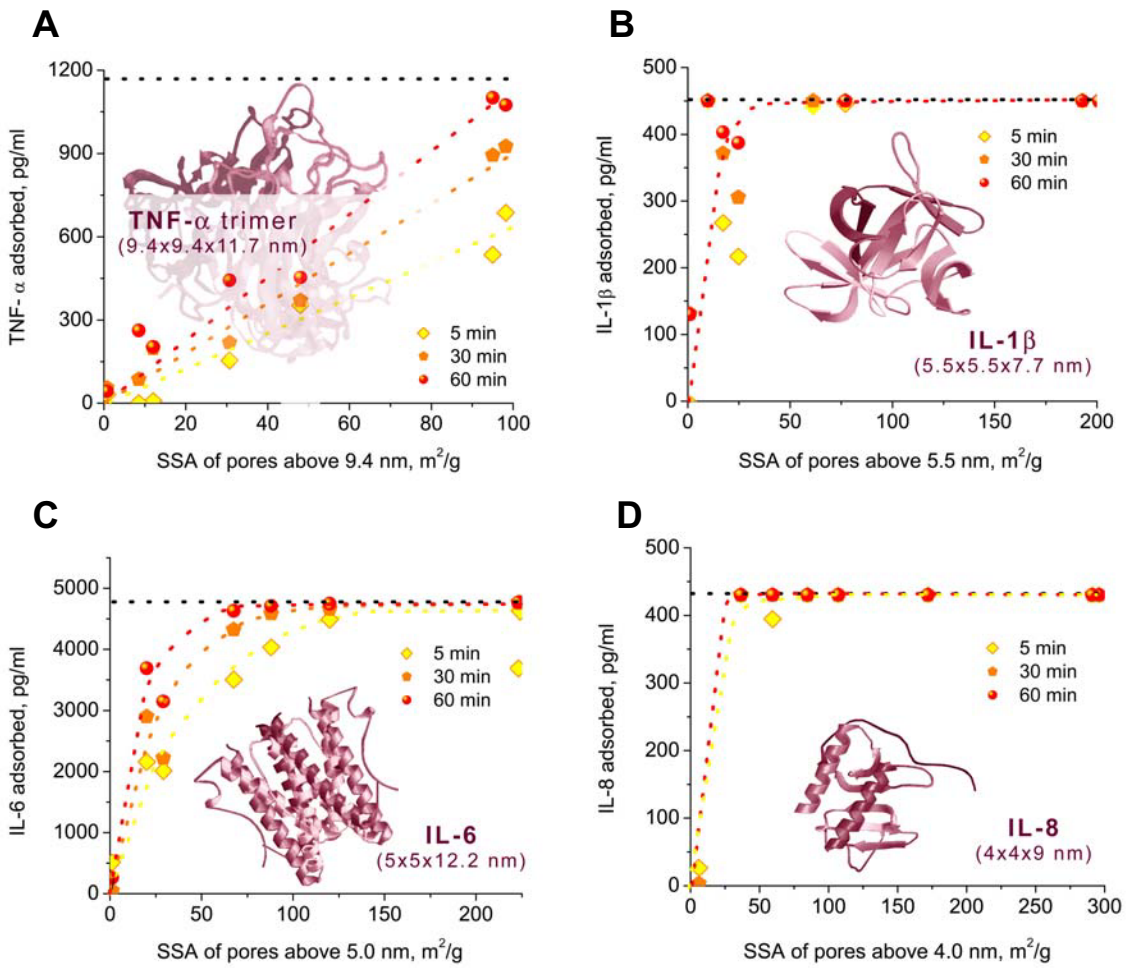

Fig. 5. Adsorption of cytokines by porous carbons as a function of the surface area accessible to the cytokines. (A) TNF-α, (B) IL-1β, (C) IL-6, (D) IL-8. The accessible area is approximated as the SSA of pores exceeding the smallest protein dimension in size: 9.4 nm for TNF-α trimer, 5.5 nm for IL-1β, 5 nm for IL-6, and 4 nm for IL-8. Amount of the adsorbed cytokines was measured after 5, 30, and 60 min adsorption. Larger carbon surface area accessible to the cytokines clearly results in faster and more complete adsorption. The horizontal dotted black line on the top of each graph indicates the initial concentration of the cytokines in plasma.

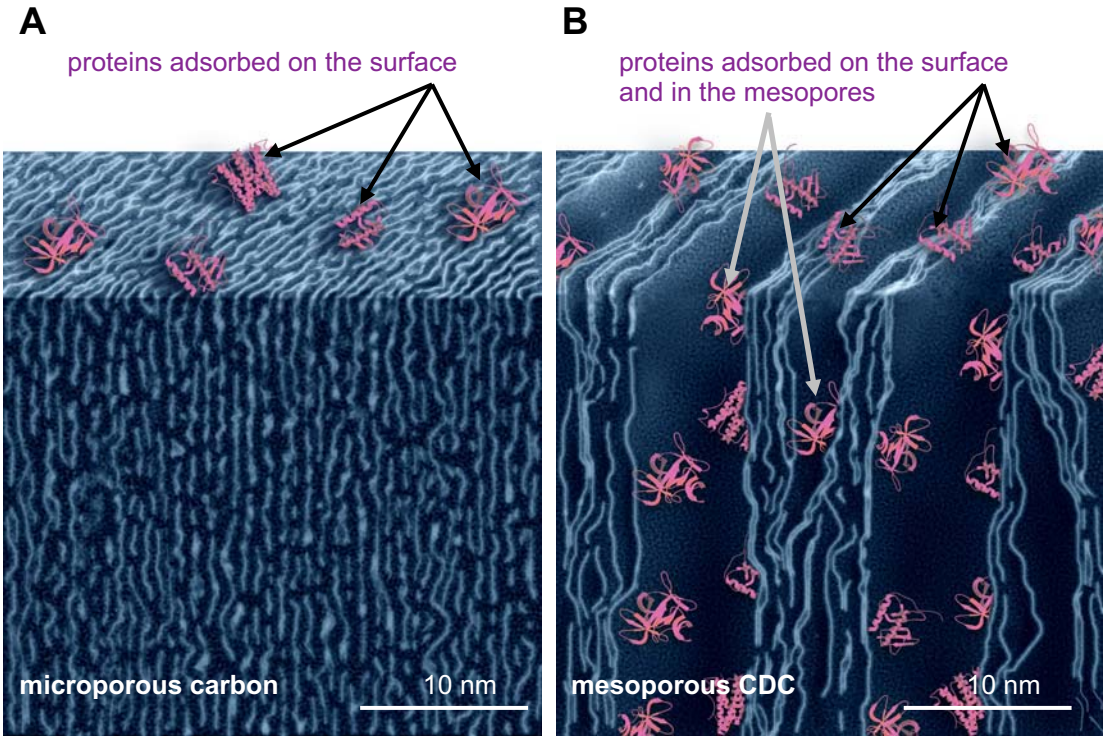

Fig. 6. Schematics of protein adsorption by porous carbons. (A) Surface adsorption in microporous carbon. Small pores do not allow proteins (shown in pink) to be adsorbed in the bulk of carbon particles (shown in blue). (B) Adsorption in the bulk of mesoroporous CDC. Large mesopores are capable to accommodate most of the proteins. Carbon particles are shown in cross-section. Alignment of the slit-shaped pores drawn in both illustrations is a simplification.

Reference

1. Slade, E., Tamber, P. S. & Vincent, J. L. (2003) *Crit. Care* **7**, 1-2.
2. Williams, M.D., Braun, L.A., Cooper, L.M., Johnston, J., Weiss, R.V., Qualy, R.L. & Linde-Zwirble, W. (2004) *Crit. Care*, **8,** R291-R298.
3. Angus, D.C., Linde-Zwirble, W.T., Lidicker, J., Clermont, G., Carcillo, J. and Pinsky, M.R. (2001) *Crit. Care Med.*, **29,** 1303-1310.
4. Asachenkov, A., Marchuk, G., Mohler, R. & Zuev, S. (1994) *IEEE Trans. Biomed. Eng.*, **41,** 943-953.
5. Callard, R., George, A. & Stark, J. (1999) *Immunity*, **11,** 507-513.
6. Neugebauer, E., Willy, C. & Sauerland, S. (2001) *Shock*, **16,** 252-258.
7. Natanson, C., Esposito, C.J. & Banks, S.M. (1998) *Crit. Care Med.*, **26,** 1927-1931.
8. Mikhalovsky, S.V. (2003) *Perfusion-UK*, **18,** 47-54.
9. Sandeman, S.R., Howell, C.A., Phillips, G.J., Lloyd, A.W., Davies, J.G., Mikhalovsky, S.V., Tennison, S.R., Rawlinson, A.P., Kozynchenko, O.P., Owen, H.L.H. *et al.* (2005) *Biomaterials*, **26,** 7124 – 7131
10. Ryoo, R., Joo, S.H. & Jun, S. (1999) *J. Phys. Chem. B*, **103,** 7743-7746.
11. Xia, Y.D. & Mokaya, R. (2004) *Adv. Mater.*, **16,** 886-891.
12. Lee, J., Han, S. & Hyeon, T. (2004) *J. Mater. Chem.*, **14,** 478-486.
13. Gogotsi, Y., Nikitin, A., Ye, H., Zhou, W., Fischer, J.E., Yi, B., Foley, H.C. & Barsoum, M.W. (2003) *Nature Mater.*, **2,** 591-594.
14. Dash, R.K., Nikitin, A. and Gogotsi, Y. (2004) *Micropor. Mesopor. Mater.*, **72,** 203-208.
15. Dash, R.K., Yushin, G., Laudisio, G., Fischer, J.E. and Gogotsi, Y. (in press, 2006) *Carbon*.
16. R. K. Dash, G. Yushin & Y. Gogotsi. (2005) *Micropor. Mesopor. Mater.*, **86**, 50-57.
17. Barsoum, B.M. & El-Raghy, T. (2001) *Amer. Scientist*, **89,** 334-343.
18. Gregg, S.J. & Sing, K.S.W. (1982) *Adsorption, Surface Area and Porosity*. Academic Press, London.
19. Ravikovitch, P.I. & Neimark, A.V. (2001) *Colloids and Surfaces*, **187–188,** 11–21.
20. Yushin, G., Gogotsi, Y. & Nikitin, A. (2006) in *Nanomaterials Handbook ed.* Gogotsi, Y. (CRC Press), pp. 237-280.
21. Reed, C., Fu, Z.Q., Wu, J., Xue, Y.N., Harrison, R.W., Chen, M.J. & Weber, I.T. (1997) *Protein Engineering*, **10,** 1101-1107.
22. Kellum, J.A., Song, M.C. & Venkataraman, R. (2004) *Crit. Care Med.*, **32,** 801-805.
23. Hinterdorfer, P., Baumgartner, W., Gruber, H.J., Schilcher, K. and Schindler, H. (1996) *Proc. Natl. Acad. Sci.* USA, **93,** 3477-3481.
24. Weber, V., Linsberger, I., Ettenauer, M., Loth, F., Hoyhtya, M. & Falkenhagen, D. (2005) *Biomacromolecules* **6,** 1864-1870.

25. Einspahr, H., Clancy, L.L., Muchmore, S.W., Watenpaugh, K.D., P. K. W. Harris, D. B. Carter, Curry, K.A., Tomich, C.-S.C., Yem, A.W., Deibel, M.R. *et al.* (1988) *J. Cryst. Growth*, **90,** 180-187.
26. Somers, W., Stahl, M. & Seehra, J.S. (1997) *Embo Journal*, **16,** 989-997.
27. Rajarathnam, K., Clarklewis, I. & Sykes, B.D. (1995) *Biochemistry*, **34,** 12983-12990.
28. Reinhart, K., Meier-Hellmann, A., Beale, R., Forst, H., Boehm, D., Willatts, S., Rothe, K.F., Adolph, M., Hoffmann, J.E., Boehme, M. *et al.* (2004) *Crit. Care Med.*, **32,** 1662-1668.
29. Cole, L., Bellomo, R., Hart, G., Journois, D., Davenport, P., Tipping, P. & Ronco, C. (2002) *Crit. Care Med.*, **30,** 100-106.
30. Fan, R., Karnik, R., Yue, M., Li, D.Y., Majumdar, A. & Yang, P.D. (2005) *Nano Lett.*, **5,** 1633-1637.
31. Barsoum, B.M. (2000) *Prog. Solid St. Chem.*, **28,** 201-281.
32. Yushin, G., Hoffman, E., Nikitin, A., Ye, H., Barsoum, M.W. & Gogotsi, Y. (2005) *Carbon*, **44,** 2075-2082.
33. Hoffman, E., Yushin, G.N., Barsoum, B.M. & Gogotsi, G. (2005) *Chem. Mater.*, **17,** 2317-2322.
34. Brunauer, S., Emmett, P. & Teller, E. (1938) *J. of Amer. Chem. Soc.*, **60,** 309–319.
35. Lowell, S. & Schields, J.E. (1998) *Powder Surface Area and Porosity*, New York.
36. Cohen, J. & Abraham, E. (1999) *J. Infect. Dis.*, **180,** 116-121.
37. Marum, S., Riberio, J.P., Arranhado, E., Lage, H., Mota, L., Marcelino, P., Fernandes, A.P., Olivera, J. & Silva, M.R. (2000) *Crit Care Med*, **4,** 66.
38. Heering, P., Morgera, S., Schmitz, F.J., Schmitz, G., Willers, R., Schultheiss, H.P., Strauer, B.E. and Gabensee, B. (1997) *Int Care Med*, **23,** 228-296.

Supplementary Figures and Tables:

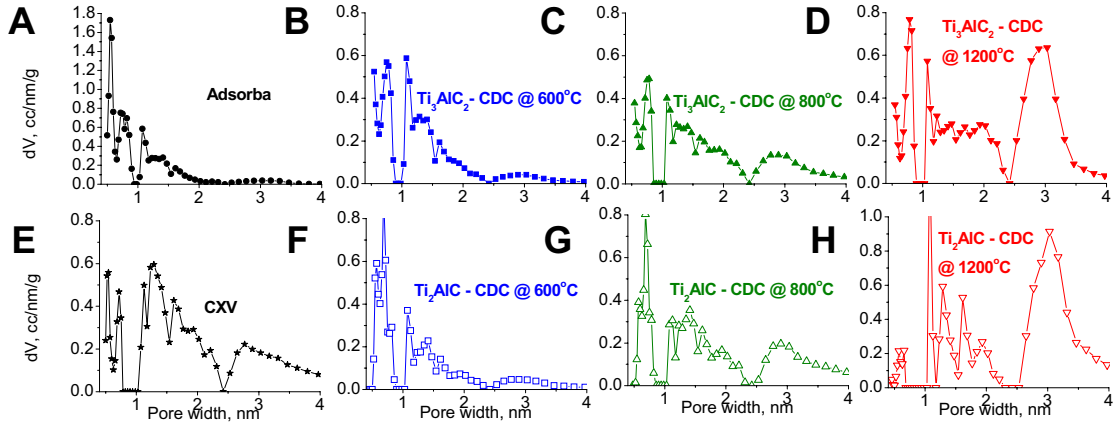

Fig. S1. Distribution of pore sizes of porous carbons in the 0.4 - 4 nm range obtained from argon sorption isotherms. (A) Adsorba, (B-D) CDC produced from Ti_3AlC_2 at 600, 800, and 1200° C, (E) CXV, (F-H) CDC produced from Ti_2AlC at 600, 800, and 1200° C. The minima at pore size of ~ 1 and 2.5 nm are artifacts of the NLDFT model.

Table.S1. Porosity of the carbon samples obtained from N_2 sorption measurements. Results are presented with respect to the samples' surface area and pore volume accessible to the cytokines to be adsorbed. Such surface area and pore volume are approximated as the SSA and volume of pores exceeding the smallest protein dimension in size: 9.4 nm for TNF-α trimer, 5.5 nm for IL-1β, 5 nm for IL-6, and 4 nm for IL-8.

	Adsorba	**CXV**	**Ti_3AlC_2-CDC, 600°C**	**Ti_3AlC_2-CDC, 800°C**	**Ti_3AlC_2-CDC, 1200°C**	**Ti_2AlC-CDC, 600°C**	**Ti_2AlC-CDC, 800°C**	**Ti_2AlC-CDC, 1200°C**
BET-SSA, m^2/g	1589	1652	1285	920	1493	1348	1649	2100
DFT-SSA, m^2/g	1362	1025	940	727	1037	1330	1412	1856
SSA of pores above 9.5 nm, m^2/g	0.76	14.6	8.53	98.2	30.7	12	95	48
SSA of pores above 5.5 nm, m^2/g	1.1	98.3	17.2	201	61.3	24.7	193	77
SSA of pores above 5.0 nm, m^2/g	1.12	120	20	223	67.6	29.1	224	88
SSA of pores above 4.0 nm, m^2/g	5.98	172	36.5	291	84.7	59.4	296	107
Total pore volume, cc/g	0.639	1.270	0.705	1.70	1.24	0.825	2.17	2.01
Volume of pores above 9.5 nm, cc/g	0.0068	0.0824	0.074	0.781	0.257	0.104	0.817	0.497
Volume of pores above 5.5 nm, cc/g	0.0081	0.377	0.105	1.163	0.370	0.152	1.2065	0.611
Volume of pores above 5.0 nm, cc/g	0.0082	0.434	0.113	1.221	0.387	0.164	1.292	0.641
Volume of pores above 4.0 nm, cc/g	0.0188	0.554	0.149	1.373	0.425	0.232	1.45	0.685